Solute segregation in metals under irradiation*

Robert A. Johnson† and Nghi Q. Lam
Materials Science Division, Argonne National Laboratory, Argonne, Illinois 60439
(Received 18 December 1975)

A kinetic model has been designed to study substitutional solute segregation during irradiation in face-centered-cubic metals. The model includes a ⟨100⟩ split interstitial binding to impurities to second-neighbor distances, vacancy binding to impurities to first-neighbor distances, and the possibility of migration of the bound complexes. Also taken into account are the effects of vacancy and interstitial diffusional encounters with impurities and spatially independent reaction terms. The resultant rate equations have been solved numerically for a thin-foil geometry as a function of time for different temperatures, defect-production rates, internal sink concentrations, foil thicknesses, defect-impurity binding energies, and initial impurity concentrations. Using parameters appropriate for Zn in Ag, significant solute segregation is found in the temperature range from $0.2\,T_m$ to $0.6\,T_m$ (T_m is the melting point). The temperature for maximum segregation is appreciably higher for heavy-ion bombardment or high-voltage-electron-microscope irradiation rates than for fast-reactor irradiation rates. It is also found that interstitials make a major contribution in the transport of solute during irradiation. The present calculations are intended to indicate the general pattern of segregation behavior and would be useful in areas of high-voltage electron microscopy, void formation, radiation-enhanced diffusion, and advanced materials development for nuclear-reactor applications.

I. INTRODUCTION

Recent transmission-electron-microscopy and Auger-spectroscopy studies of a number of metals and alloys irradiated by energetic particles have shown that interactions of radiation-induced defects with impurities and alloying elements produce significant segregation and/or the formation of second phases at grain boundaries, void surfaces, or external boundaries of the solids.[1–6] This radiation-induced segregation is of technical interest because it can affect several important surface and bulk phenomena such as preferential sputtering, blistering, diffusion of gases in the bombarded surface, void swelling, ductility, and creep by grain-boundary sliding. A broad study of kinetic segregation under irradiation may therefore provide useful input for the development of advanced materials for both liquid-metal fast-breeder reactor and controlled-thermonuclear reactor applications.

A kinetic model for the solute-segregation phenomenon was first suggested by Anthony.[7,8] He considered two mechanisms, which may oppose or supplement each other in inducing segregation, preferential flow of solute atoms in the opposite direction to the vacancy flow and "dragging" of solute atoms in the vacancy-migration direction as a result of a strong binding between vacancies and solute atoms. Recently, a more general model, which takes into account the effects of both radiation-induced vacancies and interstitials, has been proposed by Okamoto and Wiedersich.[6] Their calculations were, however, so simplified that it is impossible to study the transient effects as well as the dependence of solute segregation on the temperature and defect-production rate.

The present model and calculations have been designed for the case of annealing during irradiation of a face-centered-cubic (fcc) metal with substitutional impurities in solution. Interstitial-impurity and vacancy-impurity interactions are included as well as the possibility of migration of the bound complexes.

Many of the details of vacancy migration in the presence of impurities and the migration of the impurities have been worked out (see Howard and Lidiard,[9] Manning,[10] and LeClaire[11] for reviews). Although some of the relevant parameters are known, uncertainties still exist in applying these models to the present situation. The corresponding case of self-interstitials and impurities has not been treated. The development of equations similar to the vacancy case would be an extremely complex problem and would result in a model with numerous unknown and interrelated parameters. Even if such a model were developed, it would be difficult to obtain an insight into the resultant physical effects. The present development is basically a phenomenological model in which an attempt has been made to limit the parameters to approximations related to several physical concepts. It is the intent of the present work to determine the general solute segregation behavior by changing these physical inputs.

II. THEORY

A. Model

It is assumed in the present theoretical treatment that the self-interstitial in an fcc crystal is in the form of a ⟨100⟩ dumbbell, migrates by a nearest-neighbor 90° rotation step, as illustrated in Fig. 1, but does not rotate at a given lattice site.

The ⟨100⟩ dumbell interstitial is assumed to migrate via orthogonal jumps into nearest-neighbor positions on the (100) planes common to the dumbbell axis.[12] The vacancy is assumed to have the form of an atom missing from a lattice site and to migrate by a nearest-neighbor jump.

Interstitial-impurity binding is assumed either when the impurity is at one end of the dumbbell or when the dumbbell is at first- or second-neighbor lattice sites to the impurity. The relevant atomic configurations are shown in Fig. 2, where the solid circle is the impurity. For an impurity-solvent dumbbell, the first dissociation step will result in a "11" symmetry. Then the "21" and "22" configurations can be obtained from this "11" configuration. Binding by the "21" and "22" configurations is called a type-*a* interstitial-impurity complex. Binding with "12" symmetry leads to a type-*b* interstitial-impurity complex, which can only migrate around the impurity and thus cannot lead to impurity migration. The vacancy is assumed to be bound to an impurity when it is at a nearest-neighbor separation distance to the impurity.

For impurity migration, three atomistic effects are considered: (1) capture, (2) caging, and (3) looping.

1. *Capture*

The capture volume for interstitials by impurities is taken as 19Ω (Ω is the atomic volume) with $\frac{3}{4}$ and $\frac{1}{4}$ of this volume associated with type-*a* and type-*b* complexes, respectively ($19\Omega = \Omega$ for the impurity $+12\Omega$ for first-neighbor sites $+6\Omega$ for second-neighbor sites). The capture volume for vacancies by impurities is taken as 13Ω.

2. *Caging*

The caging effect arises from the easy migration of the impurity to symmetrically equivalent sites within a bound configuration. The basic type-*a* interstitial-impurity cage is shown in Fig. 3. The six dumbbells are symmetrically equivalent, and it is assumed that jumping between these configurations occurs more readily than partial dissociation or detrapping. Then eventually, the complex loses its initial identity, and detrapping is equally probable from any of the six sites. The

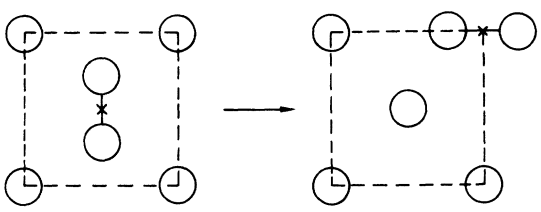

FIG. 1. ⟨100⟩ slit interstitial and its migration.

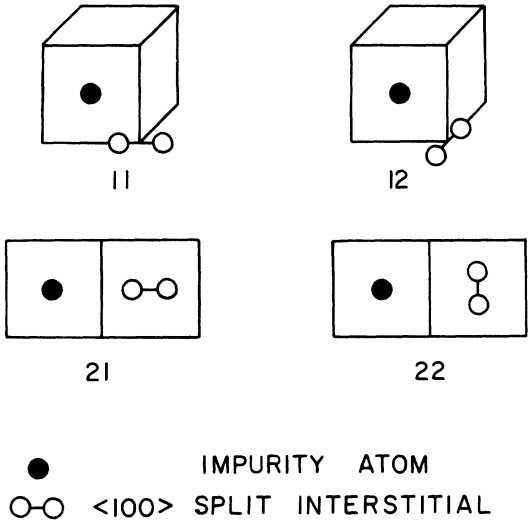

FIG. 2. Bound configurations of ⟨100⟩ slit interstitial-impurity complex.

average migration distance of the impurity within the cage is $(a/6)\times(2\sqrt{2}+1)$, almost twice the $a/2\sqrt{2}$ for a solvent–lattice-site encounter. The former value is the probability for a dumbbell to be found at any of the six symmetrically equivalent positions in the cage ($\frac{1}{6}$) times the sum of possible jump distances per caging event ($4a/\sqrt{2}+0+a$). The latter estimate is the probability ($\frac{1}{2}$) for a dumbbell to jump in one direction times the sum of jump distances ($0+a/\sqrt{2}$). The values of the average migration distances are probably overestimated because a migration of the dumbbell center (neglecting the relaxation) is consid-

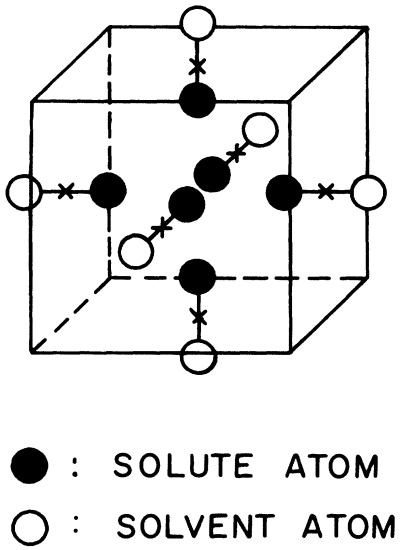

FIG. 3. Type-*a* interstitial-impurity cage.

ered in the calculations. However, the ratio of these values, which is used in the determination of σ_I and σ_v (Sec. II B) may still be accurate. Type-*b* interstitial-impurity caging is also present but has no significant consequence. Vacancy-impurity caging is simply easy back-and-forth exchange between the vacancy and the impurity that does not change the impurity-migration distance.

3. *Looping*

The looping effect, which gives rise to migration of the cages discussed above, essentially arises from a caging-type mechanism. If a type-*a* complex partially dissociates through a "11" → "21" → "11" sequence, it returns to the same basic cage from whence it originated. But if it follows a "11" → "22" → "11" sequence, a probability of $\frac{1}{2}$ exists that the center of the cage is displaced by a lattice constant a. Vacancy looping occurs when a vacancy jumps from one nearest-neighbor site to an impurity and then to another site. If caging is in effect, the net migration distance of the cage center due to such a jump is $\frac{1}{2}$ the nearest-neighbor spacing.

Capture affects the rate at which interstitial or vacancy-impurity encounters occur. Caging gives the effective impurity migration step per encounter, and looping yields the mechanism by which complexes migrate as an entity, i.e., without dissociating. The appropriate coefficients in the kinetic equations are dominated by the activation energies for various processes, for which little is known. Thus, the fine details of the Bardeen-Herring correlation are ignored.

B. Rate equations

The following reactions are included in the present formulation:

$$\text{Irradiation} \xrightarrow{K_0} C_I + C_v \,, \quad C_I + C_v \xrightarrow{K_1} 0 \,,$$

$$C_I + C_i \underset{K_2'}{\overset{K_2}{\rightleftharpoons}} C_{Iia} \,, \quad C_I + C_i \underset{K_3'}{\overset{K_3}{\rightleftharpoons}} C_{Iib} \,,$$

$$C_v + C_i \underset{K_4'}{\overset{K_4}{\rightleftharpoons}} C_{vi} \,, \quad C_I + C_{vi} \xrightarrow{K_5} C_i \,,$$

$$C_v + C_{Iia} \xrightarrow{K_6} C_i \,, \quad C_v + C_{Iib} \xrightarrow{K_7} C_i \,,$$

$$C_I + C_{Is} \xrightarrow{K_8} C_{Is} \,, \quad C_v + C_{vs} \xrightarrow{K_9} C_{vs} \,,$$

with C_I, C_v, and C_i the concentrations of free interstitials, vacancies, and impurities, respectively; C_{Iia}, C_{Iib}, and C_{vi} the concentrations of type-*a* and type-*b* interstitial-impurity and vacancy-impurity complexes, respectively; and C_{Is} and C_{vs} the effective sink concentrations for interstitials and vacancies, respectively. The rate constants are taken as

$$K_1 = 30\,(\nu_I e^{-H_I^M/kT} + \nu_v e^{-H_v^M/kT}) \,, \tag{1}$$

$$K_2 = 168\,\nu_I e^{-H_I^M/kT} \,, \tag{2}$$

$$K_2' = 4\,\nu_I e^{-(H_I^M + H_{Iia}^B)/kT} \,, \tag{3}$$

$$K_3 = 48\,\nu_I e^{-H_I^M/kT} \,, \tag{4}$$

$$K_3' = 4\,\nu_I e^{-(H_I^M + H_{Iib}^B)/kT} \,, \tag{5}$$

$$K_4 = 84\,\nu_v e^{-H_v^M/kT} \,, \tag{6}$$

$$K_4' = 7\nu_v e^{-(H_v^M + H_{vi}^B)/kT} \,, \tag{7}$$

$$K_5 = 168(\nu_I e^{-H_I^M/kT} + \nu_{vi} e^{-H_{vi}^M/kT}) \,, \tag{8}$$

$$K_6 = 126\,(\nu_v e^{-H_v^M/kT} + \tfrac{1}{7}\,\nu_{Iia} e^{-H_{Iia}^M/kT}) \,, \tag{9}$$

$$K_7 = 63\,\nu_v e^{-H_v^M/kT} \,, \tag{10}$$

$$K_8 = \alpha_I \nu_I e^{-H_I^M/kT} \,, \tag{11}$$

$$K_9 = \alpha_v \nu_v e^{-H_v^M/kT} \,, \tag{12}$$

where the ν's denote the vibration frequency factors, and H^M and H^B are the energies of migration and binding, respectively. Their values are given in Table I.

In addition, the following diffusion currents are included:

$$J_I = -\,(1 + \sigma_I C_i)\, D_I \nabla C_I \,, \tag{13}$$

$$J_v = -\,(1 + \sigma_v C_i)\, D_v \nabla C_v \,, \tag{14}$$

$$J_{Iia} = -\,D_{Iia} \nabla C_{Iia} \,, \tag{15}$$

$$J_{vi} = -\,D_{vi} \nabla C_{vi} \,, \tag{16}$$

$$J_i = \sigma_v C_i D_v \nabla C_v - \sigma_I C_i D_I \nabla C_I \,, \tag{17}$$

with the D's the appropriate diffusion coefficients,

$$D_I = \tfrac{2}{3} a^2 \nu_I e^{-H_I^M/kT} \,, \tag{18}$$

$$D_v = a^2 \nu_v e^{-H_v^M/kT} \,, \tag{19}$$

$$D_{Iia} = \tfrac{2}{21} a^2 \nu_{Iia} e^{-H_{Iia}^M/kT} \,, \tag{20}$$

$$D_{vi} = \tfrac{1}{12} a^2 \nu_{vi} e^{-H_{vi}^M/kT} \,. \tag{21}$$

D_{Iia} and D_{vi} have activation energies associated with looping, i.e., the migration energy of the complexes without dissociation. The current J_i is a consequence of the interstitial and vacancy currents, and $\sigma_I C_i$ is the ratio of the jump distance of an impurity to the jump distance of a solvent atom per encounter with an interstitial (the caging effect) times the probability of creating a type-*a* interstitial impurity complex per free interstitial jump. This probability is the concentration of impurities times a factor associated with the capture radius. And finally, this factor is taken as the ratio of the cross-sectional area of the capture volume for a type-*a* complex to that for a normal lattice atom. A similar definition is used for $\sigma_v C_i$. For strong binding, $\sigma_I = 10$ and $\sigma_v = 6$, whereas for

no interaction or repulsion, $\sigma_I = 0$ and $\sigma_v = 2$. Also, for no interaction or repulsion, the preexponential factor for D_{Iia} is reduced by a factor of $\frac{1}{6}$ to $\frac{1}{63} a^2 \nu_{Iia}$. The approximation has been made that all interstitial vibration frequency factors are the same.

Putting all the above terms together yields the following set of rate equations:

$$\frac{\partial C_I}{\partial t} = (1+\sigma_I C_i) D_I \nabla^2 C_I + \sigma_I D_I \nabla C_I \nabla C_i + K_0 - K_1 C_I C_v - K_2 C_I C_i + K_2' C_{Iia} - K_3 C_I C_i + K_3' C_{Iib} - K_5 C_I C_{vi} - K_8 C_I C_{Is} ,$$

$$\frac{\partial C_v}{\partial t} = (1+\sigma_v C_i) D_v \nabla^2 C_v + \sigma_v D_v \nabla C_v \nabla C_i + K_0 - K_1 C_I C_v - K_4 C_v C_i + K_4' C_{vi} - K_6 C_v C_{Iia} - K_7 C_v C_{Iib} - K_9 (C_v - C_v^{eq}) C_{vs} ,$$

$$\frac{\partial C_i}{\partial t} = \sigma_I C_i D_I \nabla^2 C_I + \sigma_I D_I \nabla C_I \nabla C_i - \sigma_v C_i D_v \nabla^2 C_v - \sigma_v D_v \nabla C_v \nabla C_i - K_2 C_I C_i + K_2' C_{Iia} - K_3 C_I C_i + K_3' C_{Iib} - K_4 C_v C_i + K_4' C_{vi} + K_5 C_I C_{vi} + K_6 C_v C_{Iia} + K_7 C_v C_{Iib} , \quad (22)$$

$$\frac{\partial C_{Iia}}{\partial t} = D_{Iia} \nabla^2 C_{Iia} + K_2 C_I C_i - K_2' C_{Iia} - K_6 C_v C_{Iia} ,$$

$$\frac{\partial C_{Iib}}{\partial t} = K_3 C_I C_i - K_3' C_{Iib} - K_7 C_v C_{Iib} ,$$

$$\frac{\partial C_{vi}}{\partial t} = D_{vi} \nabla^2 C_{vi} + K_4 C_v C_i - K_4' C_{vi} - K_5 C_I C_{vi} ,$$

TABLE I. Standard parameters used in the calculations.

Name of parameter	Notation	Value	Reference
Vibration frequency factor for interstitial	ν_I	10^{14} sec^{-1}	Present calculations
Vibration frequency factor for type-a interstitial-impurity complex	ν_{Iia}	10^{14} sec^{-1}	Present calculations
Vibration frequency factor for vacancy	ν_v	10^{13} sec^{-1}	Present calculations
Vibration frequency factor for vacancy-impurity complex	ν_{vi}	2.9×10^{13} sec^{-1}	15
Migration energy of interstitial	H_I^M	0.10 eV	17
Migration energy of type-a interstitial-impurity complex	H_{Iia}^M	0.22 eV	Present calculations
Binding energy of type-a interstitial-impurity complex	H_{Iia}^B	0.20 eV	Present calculations
Binding energy of type-b interstitial-impurity complex	H_{Iib}^B	0.12 eV	Present calculations
Formation energy of vacancy	H_v^F	1.00 eV	18
Migration energy of vacancy	H_v^M	0.84 eV[a]	18
Migration energy of vacancy-impurity complex	H_{vi}^M	0.88 eV	15[b]
Binding energy of vacancy-impurity complex	H_{vi}^B	0.05 eV	19
Defect-production rate	K_0	10^{-3} dpa/sec	
Foil thickness	L	10^3 Å	
Internal sink density	ρ_d	0	
Initial impurity concentration	C_i^0	10^{-3}	

[a]When a lower migration energy for vacancy $H_v^M = 0.76$ eV (Ref. 20) was used, solute segregation $\Delta C_i/C_i^0$ increased only slightly, by ~3% for $T = 300$ °C and $L = 1000$ Å due to dominant interstitial contribution.

[b]The data in Ref. 15 can be analyzed to give $H^M(w_1) - H^M(w_3) = 0.008$ eV and $H^M(w_0) - H^M(w_4) = 0.022$ eV. With the assumption $H^B = H^M(w_3) - H^M(w_4)$, $H^M(w_1) = H^M(w_0) + H^B - 0.014$ eV. $H^M(w_1)$ is the present H_{vi}^M, $H^M(w_0)$ is H_v^M, and H^B is H_{vi}^B.

with C_v^{eq} the equilibrium concentration of vacancies.

The present phenomenological approach was developed to permit straightforward variation of the primary physical effects that give rise to solute segregation under irradiation conditions. Small correlation effects, which will change from case to case and will be no larger than the unknown variations in the frequency factors, have been neglected. Given the uncertainty in the physical parameters of the model, especially since the activation energies occur in exponentials, neglect of the small correlation effects would not alter the results. The neglect of clustering is more serious. However, clustering must be neglected because these reactions (e.g., C_v+C_{vi}, $C_{vi}+C_i$, and C_v+C_v) require the introduction of additional parameters about which even less is known. Thus, the results of the calculations with this model should indicate overall trends and should clarify the effects of variation of basic physical parameters relative to solute segregation under irradiation conditions. However, these results will not offer much insight into cluster nucleation and growth. Additional effects that are not treated in the present model involve variations in migration energies with environment and the possibility of metallurgical transformations which, for example, could effectively remove solute atoms from solution and yield solute sinks. Also, although a sink-bias parameter can be introduced, one constant effective sink concentration is used.

For the present calculations, the following additional approximations are made: The sink concentrations are taken as

$$C_{Is}=C_{vs}=\rho_d\Omega^{2/3}\ , \tag{23}$$

with ρ_d the dislocation density and Ω the atomic volume. Then the factors α_I and α_v in Eqs. (11) and (12) are given by (Damask and Dienes[13])

$$\alpha_v=\frac{2\pi a^2}{\ln(R_d/R_0)\Omega^{2/3}} \tag{24}$$

and

$$\alpha_I=\tfrac{2}{3}Z_I\alpha_v\ , \tag{25}$$

where $R_d=(1/\pi\rho_d)^{1/2}$, R_0 is the dislocation core radius, and Z_I is the interstitial bias parameter.

A linear approximation is made for the interstitial energies $H_{11}^B=H_{12}^B$, $H_{21}^B=H_{22}^B$, $H_{Iia}^B-H_{11}^B=H_{11}^B-H_{21}^B$, and $H_{Iia\to 11}^M=H_{11\to 21}^M$, the migration energy of the dumbbell in successive jumps away from the impurity. Then $H_{Iib}^B=\frac{3}{5}H_{Iia}^B$, for binding $H_{Iia}^M=H_I^M+\frac{3}{5}H_{Iia}^B$ and for repulsion $H_{Iia}^M=H_I^M-\frac{1}{5}H_{Iia}^B$. In addition, if no experimental data are available for vacancy-impurity complexes, one can take $H_{vi}^M=H_v^M$ for binding and $H_{vi}^M=H_v^M-H_{vi}^B$ for repulsion.

C. Discussion

A comparison of the present approach to the more detailed theory for vacancy migration with impurities present[14] can be made. For example, Howard and Lidiard[14] give, for the total vacancy and impurity currents,

$$J_v^t=\frac{kT}{C_v}\nabla C_v(L_{aa}+2L_{ai}+L_{ii})$$
$$-\frac{kT}{C_i}\nabla C_i[L_{aa}^f(1+Z)C_i-L_{ai}-L_{ii}] \tag{26}$$

and

$$J_i^t=\frac{kT}{C_v}\nabla C_v(L_{ia}+L_{ii})-\frac{kT}{C_i}\nabla C_iL_{ii}\ , \tag{27}$$

where C_v and C_i are the concentrations of free vacancies and impurities, respectively, and the L coefficients are complex algebraic terms involving C_{vi} and various jump probabilities for a vacancy near an impurity. These equations are then cast in a form involving ∇C_v^t and ∇C_i^t, with $C_v^t=C_v+C_{vi}$ and $C_i^t=C_i+C_{vi}$, using the mass-balance or local-equilibrium relation $C_{vi}=KC_vC_i$. Using the mass-balance relation, the present model can also be cast in the form

$$J_v^t=-\frac{kT}{C_v}\nabla C_v[L_{aa}-L_{aa}^f(1+Z)C_i+3L_{ai}+2L_{ii}]$$
$$-\frac{kT}{C_{vi}}\nabla C_{vi}[L_{aa}^f(1+Z)C_i-L_{ai}-L_{ii}] \tag{28}$$

and

$$J_i^t=\frac{kT}{C_v}\nabla C_v(L_{ia}+2L_{ii})-\frac{kT}{C_{vi}}\nabla C_{vi}L_{ii}\ . \tag{29}$$

After considerable rearrangement, J_i^t is equivalent to the present form

$$J_i^t=C_i\sigma_vD_v\nabla C_v-D_{vi}\nabla C_{vi}\ , \tag{30}$$

if the correspondence is made for

$$\sigma_v=\frac{5kw_2w_3}{6w_0(w_1+w_2+\frac{7}{2}w_3)}\ , \tag{31}$$

$$D_{vi}=\frac{D_v}{12}\frac{w_2(w_1+\frac{7}{2}w_3)}{w_0(w_1+w_2+\frac{7}{2}w_3)}\ . \tag{32}$$

For the explicit case of Zn in Ag, Rothman and Peterson[15] have obtained values for these parameters from diffusion studies. The term w_2 is analogous to the looping jump frequency of the vacancy in the present model. When the Rothman-Peterson data were used in Eq. (32), the D_{vi} were found to be 0.89 smaller at 747 °C and 0.77 smaller at 880 °C than calculated with the present approach. The coefficient σ_v obtained by Howard and Lidiard is 4.40 at 747 °C and 3.94 at 880 °C. In the present model, strong vacancy-impurity interaction yields $\sigma_v=6$, and no interaction yields $\sigma_v=2$. Since

Zn in Ag is intermediate between these extremes, σ_v has been taken as 4. Thus, although the present model does not include the small temperature dependence of the more detailed theory, it is essentially equivalent. The agreement here is fortuitously close, and its extension to vacancy-impurity cases where detailed data are not available and to interstitial-impurity cases is justified.

More recently, Anthony[7] has investigated solute segregation after quenching, using the standard Howard-Lidiard equations.[14] However, he neglects the term in the impurity current that arises from the gradient of the impurity concentration, which, in the irradiation problem, plays an important role. Also, Anthony assumes that the impurity concentration is much greater than the vacancy concentration. As a result, the ratio between the impurity current and the vacancy current is independent of vacancy concentration and vacancy current. Again, these approximations are not valid for the radiation case. The effect of the approximations could be checked by means of the present model. It should be noted that, even under steady-state conditions, the mass-balance or local-equilibrium relation cannot be treated in a straightforward manner when diffusion currents or additional reactions are present.

III. NUMERICAL CALCULATIONS

A. Calculation procedure

The calculations were performed for a thin-foil geometry, as a function of time, for various parameters: temperature, defect production rate, defect-solute binding energy, foil thickness, internal sink concentration, and solute concentration.

The GEAR package of subroutines, developed at Lawrence Livermore Laboratory,[16] was used for the numerical integration of the rate equations. With the sophistication of the package, the program could be run from zero time, starting with $\Delta t = 10^{-10}$ sec, to steady state (of the order of 10^7 sec at 0 °C) within a reasonable computing time of ~3 min. Therefore, all transient effects could be studied in detail. The calculations were made for only one-half of the foil because of the symmetry of the concentration profiles. In the actual computation, this half of the foil was divided into 22 sections, corresponding to a mesh of 24 lines; lines 1 and 23 correspond to the surface and the center of the foil, respectively. Line 24 is used to set the symmetry condition at the center. The sections near the surface were taken to be small to account for stiff concentration gradients in the surface region and were larger near the center of the foil.

The starting values (at $t = 0$) used in the present calculations are

$$C_I = C_{Iia} = C_{Iib} = 0 ,$$

$$C_v = C_v^{eq} = e^{-H_v^F/kT} ,$$

$$C_{vi} = K_4 C_v^{eq} C_i^0/(K_4' + K_4 C_v^{eq}) ,$$

and

$$C_i = C_i^0 - C_{vi} ,$$

where C_i^0 is the total initial concentration of impurity atoms free and bound to vacancies.

The boundary conditions are the following for the surface (at $x = 0$):

$$\frac{\partial C_I}{\partial t} = \frac{\partial C_{Iia}}{\partial t} = \frac{\partial C_{Iib}}{\partial t} = \frac{\partial C_v}{\partial t} = 0 ,$$

$$\frac{\partial C_{vi}}{\partial t} = \frac{K_4 C_v^{eq}}{K_4'} \frac{\partial C_i}{\partial t} ,$$

and

$$\frac{\partial C_i}{\partial t} = \frac{\partial C_i^t}{\partial t} \Big/ \left(1 + \frac{K_4 C_v^{eq}}{K_4'}\right) ,$$

where $\partial C_i^t/\partial t$, the rate of change in the total (both free and bound) solute-atom concentration at the surface, is calculated from the physical condition that the total number of solute atoms is constant in the foil; and for the foil center ($x = L/2$)

$$\frac{\partial C_I}{\partial x} = \frac{\partial C_{Iia}}{\partial x} = \frac{\partial C_{Iib}}{\partial x} = \frac{\partial C_v}{\partial x} = \frac{\partial C_{vi}}{\partial x} = \frac{\partial C_i}{\partial x} = 0 .$$

The standard parameters, given in Table I, appropriate for Zn as solute in Ag, were used when the solute segregation was calculated as a function of temperature for two defect-production rates $K_0 = 10^{-3}$ and 10^{-6} displacements per atom per second (dpa/sec). Then, with $T = 300$ °C and $K_0 = 10^{-3}$ dpa/sec, the defect-solute binding energy, internal sink concentration, foil thickness, and initial solute concentration were successively changed to study their effects on segregation.

B. Results and discussion

1. *Effect of temperature*

The concentrations of point defects (C_v^c and C_I^c), solute atoms (C_i^c), and defect-solute complexes (C_{Iia}^c, C_{Iib}^c, and C_{vi}^c) at the center of the foil are shown in Figs. 4–6, as a function of irradiation time, for $K_0 = 10^{-3}$ dpa/sec at three temperatures 0, 200, and 500 °C. The solute concentration built up at the surface (C_i^s) is also included to indicate the segregation effect. The standard parameters used are given in Table I. In all three cases, solute segregation to the surface can be seen after ~0.1 sec of irradiation time. At 0 °C (Fig. 4) solute segregation reaches a maximum at $t \simeq 10^4$ sec (see also the point marked with an asterisk in Fig. 8), decreases slowly, and finally attains steady state at $t \simeq 10^7$ sec. The concentrations of vacan-

cies and vacancy-solute complexes (C_v^c and C_{vi}^c) increase to steady-state values, whereas the concentrations of interstitials and interstitial-solute complexes (C_I, C_{Iia}, and C_{Iib}) increase first and then decrease until steady state is reached. In addition, the total flux of interstitials to the foil surface is several orders of magnitude larger than the total vacancy flux for $t < 10^{-2}$ sec (Fig. 7). Then the flux J_I^t begins to decrease and J_v^t increases until they become equal at $t \simeq 10^5$ sec, at which time solute segregation decreases toward a steady-state value.

At higher temperatures, above 100 °C, the segregation increases continuously toward a maximum steady-state value (Figs. 5 and 6). The flux of interstitials to the surface is much larger than the vacancy flux for a short time (Fig. 7), but the fluxes become equal for $t > 10^{-1}$ sec.

Steady-state solute segregation at the surface, $\Delta C_i/C_i^0 = (C_i^s - C_i^0)/C_i^0$, is plotted as a function of temperature in Fig. 8. The numbers on the curve are the times required to attain steady state at a particular $K_0 = 10^{-3}$ dpa/sec. The segregation occurs within the temperature range from $0.2T_m$ to $0.6T_m$, with a maximum around 300 °C, under heavy-ion or high-voltage electron-microscope irradiation conditions ($K_0 = 10^{-3}$ dpa/sec). The segregation is drastically reduced at higher temperatures ($T > 400$ °C), where defect-solute binding is weak and the diffusion of solute atoms from the surface due to a large solute concentration gradient becomes important. At low temperatures ($T < 100$ °C), the mutual recombination of vacancies and interstitials

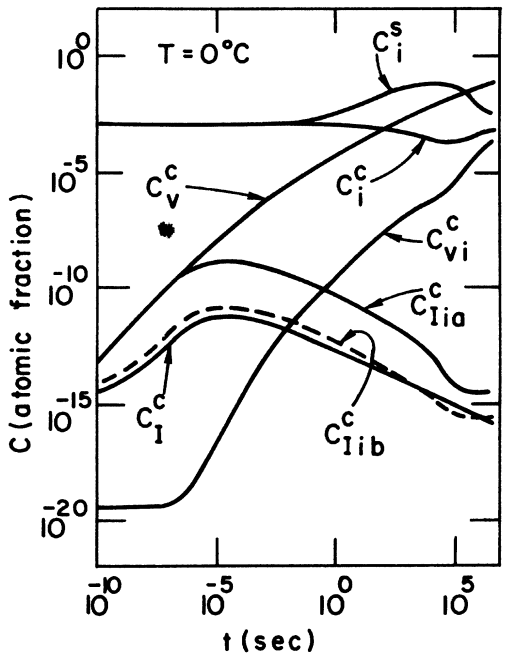

FIG. 4. Concentrations of point defects, defect-solute complexes, and solute atoms at the center of a foil irradiated at 0 °C as a function of irradiation time. Surface concentration of solute is also shown to indicate the effect of segregation.

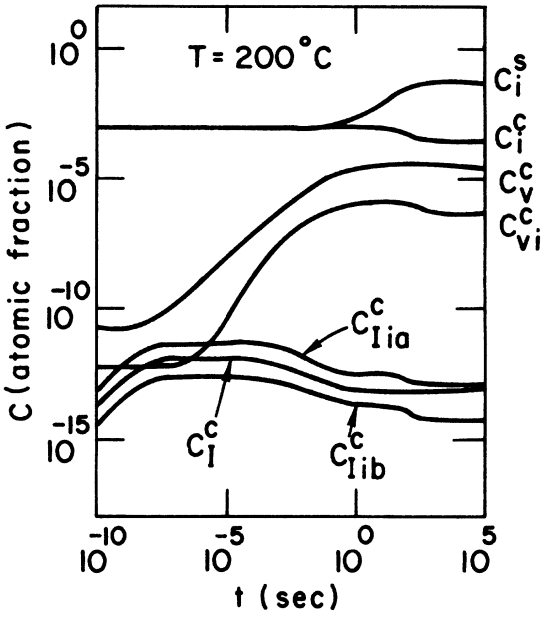

FIG. 5. Concentrations of point defects, defect-solute complexes, and solute atoms at the center of a foil irradiated at 200 °C as a function of irradiation time. Surface concentration of solute is also plotted to show the segregation effect.

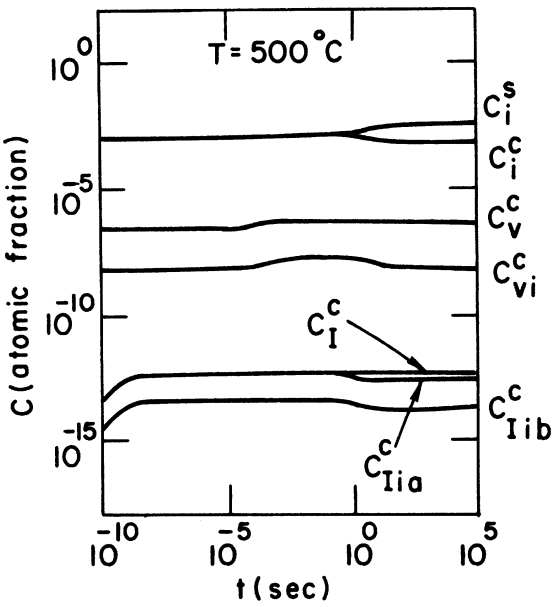

FIG. 6. Concentrations of point defects, defect-solute complexes, and solute atoms at the center of a foil irradiated at 500 °C as a function of irradiation time. Solute concentration at the surface is also shown.

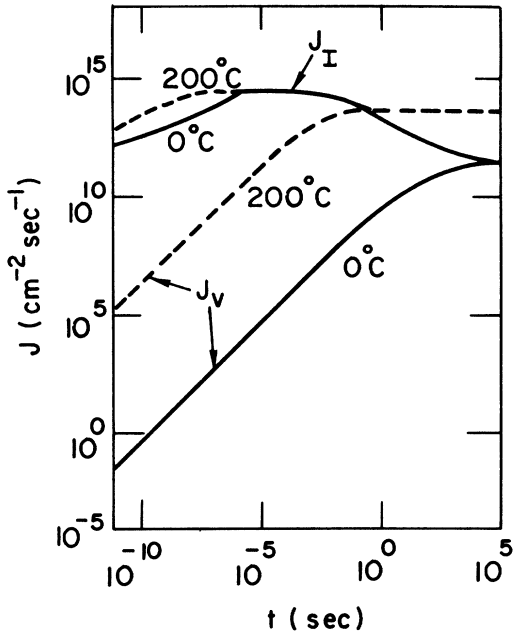

FIG. 7. Fluxes of interstitials and vacancies to the foil surface as a function of irradiation time at different temperatures.

becomes so dominant that long-range migration of point defects and defect-solute complexes is considerably reduced and solute segregation becomes negligible. The temperature dependence of the segregation found in the present calculations is similar to the case of void swelling observed experimentally.[21–24] Since impurity segregation is a phenomenon of technical interest, systematic experimental studies of the temperature dependence of segregation are highly recommended.

2. *Spatial dependence of concentrations*

Steady-state concentrations of point defects, defect-solute complexes, and solute atoms are plotted in Figs. 9–11, as a function of distance from the surface of a foil 1000 Å thick, for temperatures of

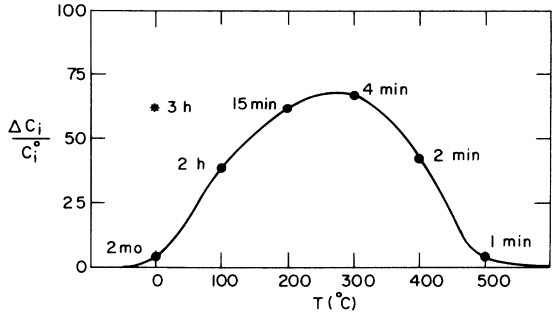

FIG. 8. Temperature dependence of steady-state solute segregation.

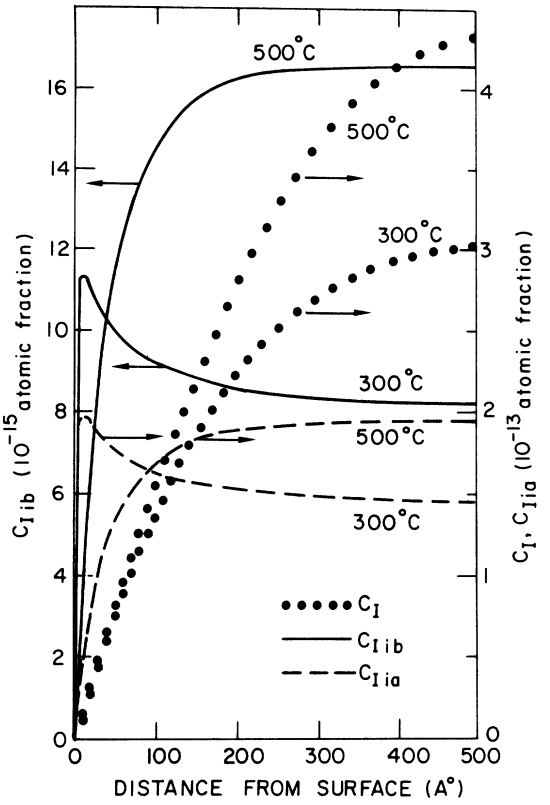

FIG. 9. Steady-state concentrations of interstitials and interstitial-solute complexes as a function of distance from a foil surface.

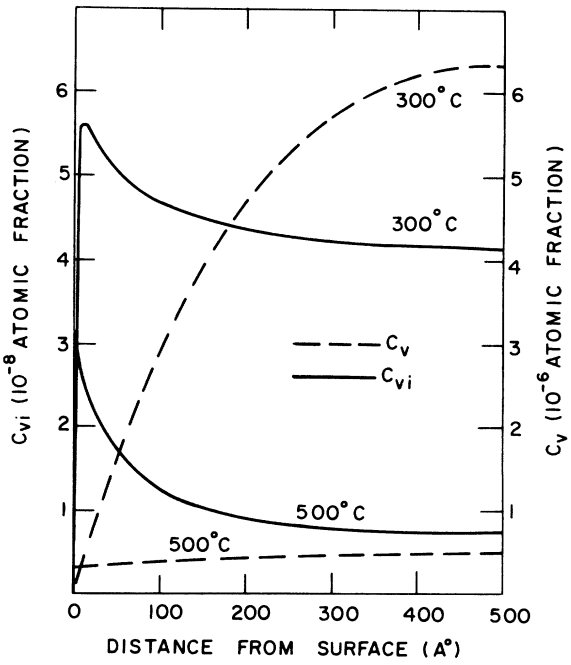

FIG. 10. Steady-state concentrations of vacancies and vacancy-solute complexes as a function of distance from a foil surface.

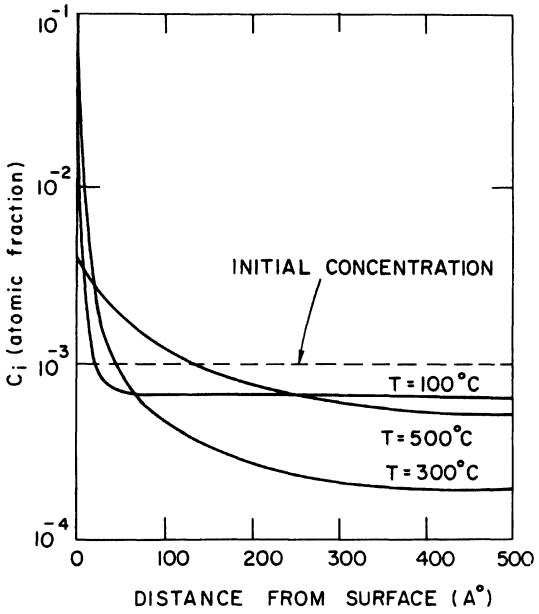

FIG. 11. Steady-state concentration of solute atoms as a function of distance from a foil surface.

300 and 500 °C. Humps are observed on the steady-state concentration profiles near the surface for defect-solute complexes at temperatures below ~ 300 °C. These humps are quite similar to those found for vacancy clusters,[25] which indicates that treating the local equilibrium near a sink is not straightforward, especially in the multireaction case.

Figure 11 shows some typical segregation profiles calculated for $T = 100$, 300, and 500 °C. Segregation is maximum at ~ 300 °C for $K_0 = 10^{-3}$ dpa/sec. In addition, the effects of backward diffusion due to a large solute-concentration gradient can also be seen; this effect tends to reduce the segregation at high temperatures.

3. *Effect of defect-production rate*

Two defect-production rates, $K_0 = 10^{-3}$ and 10^{-6} dpa/sec, corresponding to heavy-ion or high-voltage electron-microscope irradiation and fast-reactor irradiation rates, respectively, were used in the present calculations. The K_0 dependence of solute segregation is illustrated in Fig. 12, as a function of temperature for a foil 1000 Å thick. For a fixed temperature, the time required to attain steady-state segregation is much longer for $K_0 = 10^{-6}$ than for $K_0 = 10^{-3}$ dpa/sec. The segregation curve for $K_0 = 10^{-6}$ dpa/sec is shifted by ~ 150 °C to lower temperatures, relative to the curve for $K_0 = 10^{-3}$ dpa/sec. This temperature shift can be associated with the ineffective mutual recombination of vacancies and interstitials in the low-defect-production-rate case. In fact, at a low rate of defect production, point defects have a greater chance of making long-range migration to sinks or surfaces, which is essential to the segregation of solute atoms. The K_0 dependence of the steady-state mutual recombination rate at the center of the foil and the steady-state flux of vacancies and interstitials, calculated as a function of temperature, show the same temperature shift (of ~ 150 °C).

We emphasize, from the results obtained here, that in interpreting radiation-enhanced impurity diffusion data, one should keep the segregation effect in mind because, within the range of temperature and defect-production rate of interest to enhanced-diffusion experiments, impurity segregation to extended sinks may be significant.

4. *Effect of binding energies*

The dependence of solute segregation on the interstitial-solute and vacancy-solute binding energies has been studied for $T = 300$ °C, $K_0 = 10^{-3}$ dpa/sec, and $L = 1000$ Å. Several cases have been considered; the results are listed in Table II. It is found that the interstitial mechanism is dominant in the transport of solute atoms in a solid under irradiation. Solute enrichment at the surface is observed with (a) $H^B_{Iia} = H^B_{vi} = 0$, (b) $H^B_{Iia} > 0$ and $H^B_{vi} > 0$, and (c) $H^B_{Iia} > 0$ and $H^B_{vi} < 0$, whereas solute depletion occurs when (a) $H^B_{Iia} \leq 0$ and $H^B_{vi} < 0$, and (b) $H^B_{Iia} \leq 0$ and $H^B_{vi} > 0$. The significance of these results is discussed in Sec. III B8.

The effect of defect-solute binding energies is also shown in Fig. 13, where one of the binding energies is kept constant, at an appropriate value, and the other changes. With H^B_{vi} held at 0.05 eV, solute segregation increases rapidly as H^B_{Iia} increases. However, with H^B_{Iia} kept at 0.2 eV, segregation is reduced by increasing H^B_{vi} because of less efficient interstitial contribution. In fact, when vacancy-solute binding energy is high, more solute atoms are bound to vacancies, and therefore

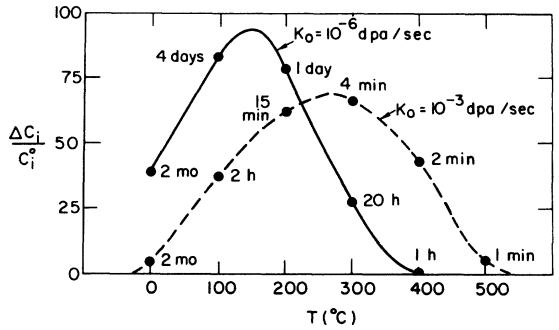

FIG. 12. Effect of defect-production rate on the temperature dependence of solute segregation.

TABLE II. Effect of defect-solute binding energies on segregation.

H^B_{Iia} (eV)	H^B_{vi} (eV)	$\Delta C_i/C_i^0$	Remarks
0.20	−0.05	137.0	Enrichment
0.20	0.00	92.9	Enrichment
0.20	0.05	66.7	Enrichment
0.20	0.10	54.6	Enrichment
0.10	0.05	38.3	Enrichment
0.00	−0.05	−0.68[a]	Depletion
0.00	0.00	0.48	Slight enrichment[b]
0.00	0.05	0.45	Slight enrichment[b]
0.00	0.20	−0.56[a]	Depletion
0.00	0.40	−0.53[a]	Depletion
−0.10	−0.05	−0.96[a]	Depletion
−0.10	0.05	−0.25[a]	Depletion

[a]With the definition of $\Delta C_i/C_i^0$ given in Sec. III B1, one should keep in mind that $\Delta C_i/C_i^0 = -1.0$ means a complete depletion of solute atoms at the surface.

[b]See discussion in Sec. III B8.

the number of free solute atoms migrating to the surface via the dominant interstitial mechanism is smaller.

5. *Effect of foil thickness*

Since the thickness of the foil affects both the concentrations of mobile defects and the buildup time to steady state, its effect on solute segregation has been studied for $T = 300\,^\circ\text{C}$, $K_0 = 10^{-3}$ dpa/sec, $C_s = 0$, and $C_i^0 = 10^{-3}$. The concentration of solute is plotted versus the distance from a foil surface in Fig. 14 for different foil thicknesses. The depth of the solute-enriched zone (where $C_i > 10^{-3}$) increases and approaches a constant value of ~170 Å for foils thicker than 8000 Å. The time required to attain a steady-state segregation is also given in Fig. 14; the thicker the foil the longer the buildup time to steady-state, as anticipated from the calculation of

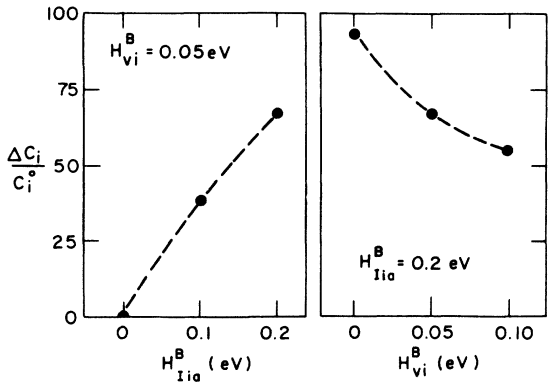

FIG. 13. Effect of defect-solute binding energies on solute segregation at 300 °C.

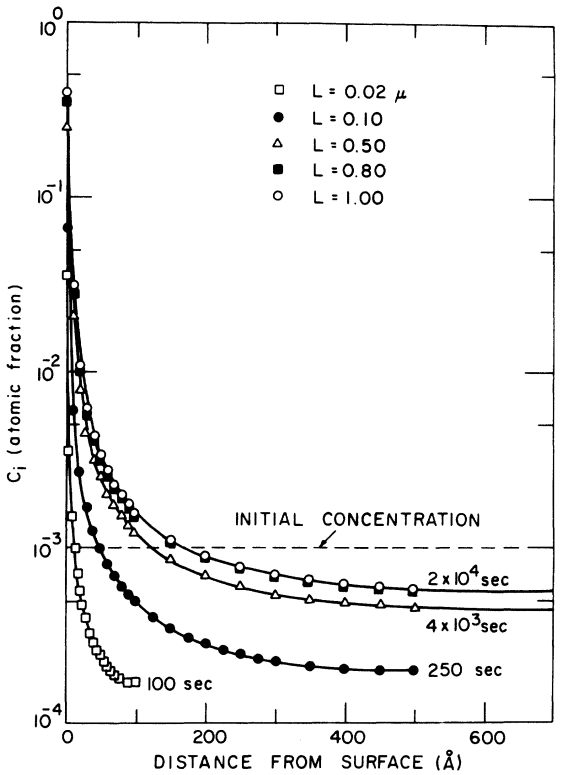

FIG. 14. Solute concentration as a function of distance from surface for different foil thicknesses.

equivalent internal sink efficiency of the surfaces.[26] The buildup time is, however, the same for foils thicker than 8000 Å. Thus, an 8000-Å-thick foil may be a good approximation of a semi-infinite medium in the study of solute segregation at 300 °C.

6. *Effect of internal sink density*

Steady-state concentrations of solute atoms at the foil surface are given in Table III for various dislocation densities in foils 1000 Å and 1 μm thick at 300 °C. Solute segregation is insensitive to dislocation densities less than the equivalent internal

TABLE III. Effect of internal sink density on segregation.

Foil thickness L (μm)	Sink density ρ_d (cm^{-2})	Interstitial bias Z_I	$\frac{\Delta C_i}{C_i^0}$
0.1	0	1.0	66.7
0.1	10^8	1.0	66.7
0.1	10^{11}	1.0	64.8
0.1	10^{11}	1.1	63.6
1.0	0	1.0	401.2
1.0	10^8	1.0	401.1
1.0	10^{12}	1.0	104.9
1.0	10^{12}	1.1	91.7

sink efficiency of surfaces,[26] $\rho_d \simeq \pi^2/L^2$ cm^{-2}. In addition, the interstitial bias also produces a small effect on segregation; for example, a bias parameter $Z_I = 1.10$ reduces the surface solute concentration by ~ 13% for $\rho_d = 10^{12}$ cm^{-2} and $L = 1$ μm.

7. *Effect of initial solute concentration*

Two initial solute concentrations, $C_i^0 = 10^{-3}$ and 10^{-5}, were considered in the present calculations. A comparison of $\Delta C_i/C_i^0$ is made in Table IV for various temperatures with $K_0 = 10^{-3}$ dpa/sec and $L = 1000$ Å. The values of $\Delta C_i/C_i^0$ are slightly smaller for $C_i^0 = 10^{-5}$ than for $C_i^0 = 10^{-3}$. However, the temperature dependence of solute segregation is unchanged; maximum segregation is still observed around 300 °C.

8. *Accuracy of calculations*

The accuracy of the present calculations is affected by both mathematical and physical approximations (in addition to the assumptions discussed relative to the development of the model). The distance-mesh size is $\Delta x = 10$ Å near the surface of foils of thickness ≥ 1000 Å. Even with this small size, the slope of the concentration curves can change sufficiently from point to point, which introduces an error in the calculations of the slopes and curvatures at these points. In addition to this strictly mathematical error, these rapidly changing conditions also introduce a physical ambiguity into the model relative to the use of continuum concentrations to describe an atomistic situation. For instance, the probability of a vacancy encountering a solute atom actually depends on the concentration of solute atoms in the direction the vacancy is jumping, not at its present location. The assumption in going from atomistic considerations to continuum equations, that the concentration gradients change slowly relative to the jump distance, is not too accurate in the present case.

An additional factor that can introduce errors involves the approximation that the foil thickness remains constant. This essentially gives rise to a situation involving nonconservation of the number of atoms. As vacancy concentrations build up relative to interstitial concentrations, more interstitials than vacancies arrive at the surface, and some swelling of the sample occurs. The approximation used here yields a slight segregation effect; an interstitial disappears when it reaches the surface, whereas a solute atom is retained there.

The flux of vacancies and interstitials to the surface, for a sink bias parameter of $Z = 1.0$, should be equal at steady state. As a consequence of the sources of error discussed above, the fluxes are found to be approximately but not exactly equal. The effect of this discrepancy is negligible when segregation effects are large, but it can be significant when the segregation is small. For example, no segregation should occur when $H_{Iia}^B = H_{vi}^B = 0$. The slight enrichment listed in Table II for this case is therefore not physically significant. The values listed indicate that the small segregation effects are minor and also show the relative effects for these cases (the errors discussed here should enter the different calculations in approximately the same way). The magnitude of this error is negligible on the scale of segregation plotted in Fig. 12.

TABLE IV. Effect of initial solute concentration on segregation.

Temperature T (°C)	Initial solute concentration C_i^0	$\Delta C_i/C_i^0$
100	10^{-5}	35.8
	10^{-3}	38.2
200	10^{-5}	56.0
	10^{-3}	61.6
300	10^{-5}	60.9
	10^{-3}	66.7
400	10^{-5}	44.0
	10^{-3}	42.5

IV. CONCLUSIONS

Solute segregation in an fcc metal foil under irradiation has been modeled and studied as a function of irradiation temperature, defect-production rate, defect-solute binding energy, foil thickness, internal sink density, and initial solute concentration. Using parameters appropriate for Zn in Ag, significant solute segregation is found in the temperature range from $0.2T_m$ to $0.6T_m$. Maximum segregation is observed around $0.45T_m$ for a defect-production rate of 10^{-3} dpa/sec. However, the temperature for maximum segregation is appreciably lower for fast-reactor irradiation rates than for heavy-ion bombardment or high-voltage electron-microscope irradiation rates.

Solute migration to a foil surface by the interstitial mechanism is dominant in the segregation process. With an interstitial-solute binding energy of 0.2 eV, solute segregation is found to decrease as the vacancy-solute binding energy increases. This can be interpreted in terms of a decrease in the number of unbound solute atoms that can participate in the interstitial dragging process.

The internal sink concentration only affects the solute segregation to the surface if, for a given foil thickness, it is higher than the equivalent internal sink efficiency of the surfaces. The initial solute concentration does not appreciably affect the quantity $\Delta C_i/C_i^0$, which is a measure of surface segregation.

The present calculations show that solute segregation may be so significant at temperatures below $\sim 0.5T_m$ that all the radiation-enhanced impurity-diffusion data must be interpreted with great care.

ACKNOWLEDGMENTS

The authors wish to thank Dr. H. Wiedersich and Dr. P. R. Okamoto for their interest and fruitful discussions throughout various phases of the present work, Dr. G. Leaf and Dr. G. D. Byrne for their help with the GEAR subroutine, and Dr. N. L. Peterson and Dr. R. W. Siegel for commenting on the manuscript. One of the authors (R. A. J.) is grateful to the National Science Foundation and Argonne Center for Educational Affairs for support during his stay at Argonne National Laboratory.

Note added in proof: Following a suggestion by W. Schilling, Mössbauer-spectroscopy data for Co in irradiated Al have been interpreted by Vogl, Mansel, and Dederichs in terms of the same caging mechanism assumed for the type *a* self-interstitial-impurity configuration in the present paper.

---

*Work supported by the U. S. Energy Research and Development Administration.

†Visiting scientist from Materials Science Department, University of Virginia, Charlottesville, Virginia 22901.

[1]P. R. Okamoto, S. D. Harkness, and J. J. Laidler, ANS Trans. 16, 70 (1973).

[2]P. R. Okamoto, A. T. Santhanam, H. Wiedersich, and A. Taylor, Nucl. Technol. 22, 45 (1974).

[3]A. T. Santhanam, A. Taylor, and S. D. Harkness, Nucl. Met. 18, 302 (1973).

[4]H. Shiraishi, P. R. Okamoto, and A. Taylor (unpublished).

[5]T. Ryan, Ph. D. thesis (University of Michigan, Ann Arbor, 1975) (unpublished).

[6]P. R. Okamoto and H. Wiedersich, J. Nucl. Mater. 53, 336 (1974).

[7]T. R. Anthony, in *Atomic Transport in Solids and Liquids*, edited by A. Lodding and T. Lagerwall (Verlag Z. Naturforch., Tübingen, Germany, 1971), p. 138.

[8]T. R. Anthony, in *Radiation-Induced Voids in Metals and Alloys*, edited by J. W. Corbett and L. C. Ianniello, AEC Symp. Series, Conf.-701601 (U. S. A. E. C. Technical Information Center, Oak Ridge, Tennessee, 1972), p. 630.

[9]R. E. Howard and A. B. Lidiard, Rep. Prog. Phys. 27, 161 (1964).

[10]J. R. Manning, *Diffusion Kinetics for Atoms in Crystals* (Van Nostrand, Princeton, 1968), p. 75 ff.

[11]A. D. LeClaire, in *Physical Chemistry*, edited by W. Jost (Academic, New York, 1970), p. 261.

[12]R. A. Johnson, Phys. Rev. 145, 423 (1966).

[13]A. C. Damask and G. J. Dienes, *Point Defects in Metals* (Gordon and Breach, New York, 1963), p. 78.

[14]R. E. Howard and A. B. Lidiard, Philos. Mag. 11, 1179 (1965).

[15]S. J. Rothman and N. L. Peterson, Phys. Rev. 154, 552 (1967).

[16]A. Hindmarsh, Lawrence Livermore Laboratory Report UCID-30001, 1974 (unpublished).

[17]K. Herschbach, Phys. Rev. 130, 554 (1963).

[18]H. Mehrer and A. Seeger, Phys. Status Solidi 39, 647 (1970).

[19]R. W. Balluffi and P. S. Ho, *Diffusion* (American Society for Metals, Metals Park, Ohio, 1972), p. 83.

[20]Nghi Q. Lam, S. J. Rothman, H. Mehrer, and L. J. Nowicki, Phys. Status Solidi B 57, 225 (1973).

[21]Y. Adda, in Ref. 8, p. 31.

[22]J. L. Brimhall, H. E. Kissinger, and G. L. Kulcinski, in Ref. 8, p. 338.

[23]G. L. Kulcinski, J. L. Brimhall, and H. E. Kissinger, in Ref. 8, p. 449.

[24]S. D. Harkness and C. Y. Li, in Ref. 8, p. 798.

[25]Nghi Q. Lam, J. Nucl. Mater. 56, 125 (1975).

[26]G. J. Dienes and G. H. Vineyard, *Radiation Effects in Solids* (Interscience, New York, 1957), p. 142.